Nanometer-Scale Optical Imaging of Epitaxially Grown GaN and InN Islands Using Apertureless Near-Field Microscopy†

Zee Hwan Kim, Bing Liu, and Stephen R. Leone*

Department of Chemistry and Physics, University of California, and Lawrence Berkeley National Laboratory, Berkeley, California 94720

Received: June 15, 2004

Nanometer-scale chemical imaging of epitaxially grown gallium nitride (GaN) and indium nitride (InN) islands is performed using scattering-type apertureless near-field scanning optical microscopy (ANSOM). The scattering of 633 nm laser radiation is modulated by an oscillating metallic probe, and the scattered radiation is detected by homodyne amplification, followed by high-harmonic demodulation, yielding optical near-field scattering maps with a spatial resolution better than 30 nm. The image contrast between InN and GaN, and the tip−sample distance dependence, can be qualitatively explained by a simple dipole-coupling model. The ANSOM images of InN and GaN also show structures that are absent in the topographic counterpart, and these substructures are explained by the variations of the local dielectric environment of InN and GaN.

Introduction

Rapid progress in materials science and nanotechnology relies heavily on the characterization of mesoscopic properties of materials, which demands microscopy techniques that are able to map out the chemical/physical environment with nanometer resolution. Unfortunately, conventional far-field optical microscopy is limited by the diffraction of light and cannot provide resolution better than half of the wavelength (∼300 nm) of the light employed. The recently developed near-field scanning optical microscopy (NSOM) technique based on the metal-clad fiber probe offers resolution below the diffraction limit,[1−3] but the practical resolution is limited to 60−100 nm[4] because of the finite skin depth of the metal coating and the low optical transmission of the probe. Also, the accessible wavelengths are limited by the optical absorption of the materials used for the probe.

More recently, Keilmann and co-workers[5,6] and Wickramasinghe and co-workers[7] introduced a radically different NSOM technique based on the local field enhancement and light scattering by "apertureless" probes (sharp metallic or dielectric scanning probe tips). The probe in near contact with the sample is externally illuminated by a focused laser beam, and scattered light is recorded as a function of the sample position. The scattering from the probe depends sensitively on the presence of the nearby sample because of the mutual perturbations of the polarizabilities of the probe and sample. In principle, the resolution of the apertureless NSOM (ANSOM) is only limited by the radius of curvature of the probe, and it yields superior resolution (<30 nm) compared with that of conventional NSOM. Because the probe is externally illuminated by a focused laser beam, wavelength restrictions and low-transmission problems are alleviated as well. Currently, a variety of related apertureless microscopy techniques, combining linear and nonlinear spectroscopy and field enhancement, are being investigated.[8−11] Even though the original concept of ANSOM is simple, the detailed nature of the image-formation mechanism (including details such as probe−sample coupling, the effects of sample topography, and the degree of field localization) is largely unknown, and further experimental and theoretical efforts are needed to refine the ANSOM technique for more routine and quantitative application.

Here, we report the nanometer-scale optical imaging of gallium nitride (GaN) and indium nitride (InN) islands using the ANSOM technique. Group III nitride semiconductors are receiving a great amount of attention because of their applicability to blue/UV optoelectronic devices, such as light-emitting diodes and quantum-well lasers.[12] In addition to measurements of bulk dielectric parameters (such as refractive indices and extinction coefficients), evaluation of physical defects and chemical inhomogeneities will greatly help to optimize device performance. The development of selective optical techniques to excite or probe these materials on nanometer-length scales will greatly aid in the ability to characterize them. High-resolution ANSOM imaging of the nitride semiconductors can allow us to understand the impact of the local inhomogeneity on the performance of UV optoelectronic devices. In this work, we explore the nanometric optical mapping of epitaxially grown InN and GaN islands using the scattering-type ANSOM and interpret the image contrast in the framework of dipole coupling between the metallic tip and the sample.

Detection of the Near-Field Scattering

To correctly extract the near-field scattering component, the following three techniques are combined in this work: side illumination, high harmonic demodulation, and homodyne amplification by an external interferometer.[5,6,13]

For the optimal field enhancement at the end of the metallic probe, the polarization direction of the excitation field should be parallel to the major axis of the tip.[14,15] The side-illumination scheme allows convenient access to the desired parallel polarization. In ANSOM, a vertically oscillating tip (perpendicular to the sample surface with frequency Ω) in near contact with the sample is *externally* illuminated by a focused laser beam. The illuminated area around the probe is much larger than the

† Part of the special issue "George W. Flynn Festschrift".

* Corresponding author: srl@uclink.berkeley.edu.

10.1021/jp047425i CCC: $30.25
Published on Web 01/25/2005

size of the probe (~1 μm in diameter for the diffraction-limited spot versus 30 nm of the AFM tip). Inevitably, the collected scattered field (E_{SC}) is dominated by the (far-field) background that originates from the reflections from the sample and the oscillating cantilever, and this background *coherently* adds to the near-field component (E_{NF}) of the signal:

$$E_{SC}(\Omega) = E_{NF}(\Omega) + E_T(\Omega) + E_S \quad (1)$$

where the E_S and $E_T(\Omega)$ are the constant (surface reflection) and modulated (tip reflection) components of the far-field background, respectively. Noting that E_S is the dominant component of the detected field ($|E_S|$, $|E_{NF}|$, and $|E_T|$), the signal intensity registered by the detector/lock-in amplifier, $S_{n\Omega}$, is given as

$$S_{n\Omega} \sim |E_{NF,n\Omega}||E_S| \cos \Delta + |E_{T,n\Omega}||E_S| \cos \Phi \quad (2)$$

where $n\Omega$ represents the nth harmonic Fourier component of the probe oscillation, Ω, and Δ and Φ are the relative phases of E_{NF} and E_T with respect to E_S, respectively. The second term in eq 2 represents the interference between the far-field backgrounds that leads to image artifacts. Because of the strongly anharmonic response of E_{NF} with respect to the harmonic oscillation of the probe, compared to the nearly harmonic response of E_T, this background term can be selectively removed by recording the signal at the higher harmonics (2Ω, 3Ω, ...) of the probe oscillation:[16,17]

$$S_{n\Omega} \sim |E_{NF,n\Omega}||E_S| \cos \Delta \qquad (n \geq 2) \quad (3)$$

The relative phase between E_{NF} and E_S, Δ, is ill-defined, and it has been shown to cause serious topographic artifacts in ANSOM images as well.[6,18] By coherently mixing E_{SC} in eq 1 with a stronger reference beam (E_{ref}) that has a well-defined phase (homodyning), we can override the interference between E_{NF} and E_S with the stronger interference between E_{NF} and E_{ref} to obtain a nonambiguous, artifact-free signal:

$$S_{n\Omega} \sim |E_{NF,n\Omega}||E_{ref}| \cos \Gamma \propto |E_{NF,n\Omega}| \cos \Gamma \quad (4)$$

where Γ denotes the phase difference between the near field and the reference field. This homodyne amplification by an external reference beam removes topographic artifacts and drastically improves the signal-to-noise ratio. In the following, all of the results shown are from the homodyne-amplified signals.

Experimental Procedure

Our setup is a combination of a home-built tapping-mode atomic force microscope (AFM) and a Michelson interferometer (see Figure 1). The AFM tips used are commercially available, standard etched Si tips, coated with platinum and titanium (NSC15/Ti−Pt, MikroMasch). The tip has a nominal radius of curvature of less than 50 nm. The AFM probe oscillates near the natural resonance frequency of the cantilever ($\Omega \sim 300$ kHz) with an amplitude of ~20 nm above the sample surfaces. During scanning (PI-500, PI-Polytech) of the sample, a feedback loop maintains a constant tip−sample distance by vertically displacing the sample. The feedback loop usually operates in the soft-tapping (small-damping) condition.

The output beam of an intensity-stabilized He−Ne laser (Micro-g Inc., 1 mW) is spatially filtered and expanded in size before being introduced to the input port of the interferometer. A half-wave plate (CVI) ensures the polarization of the input

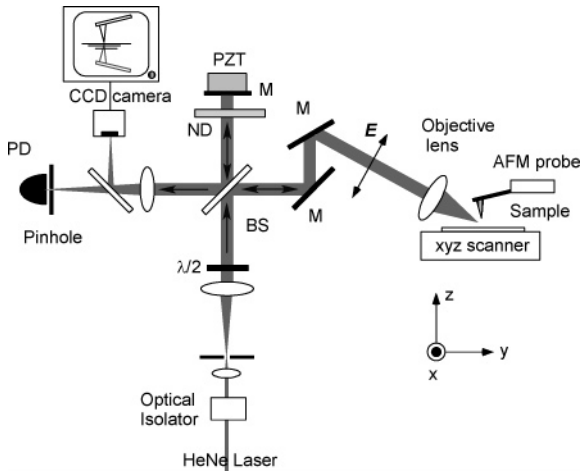

Figure 1. Experimental setup for the ANSOM: M = mirror, PD = photodiode, ND = neutral density filter, PZT = pzt transducer, BS = 50:50 beam splitter, and $\lambda/2$ = half-wave plate. The CCD camera is for alignment. The coordinate system (x, y, z) for illumination is shown by arrows.

beam to be parallel to the axis of the AFM probe. In one arm of the interferometer (reference beam), a mirror mounted on the computer-controlled piezo-stack transducer (Thorlabs) retroreflects the beam onto the output port of the interferometer. The beam in the other arm of the interferometer is directed to the input aperture of a microscope objective lens (Mituyo, long working distance model, 0.22 NA) and consequently focused onto the tip−sample junction with an angle of ~30° with respect to the sample surface. Backscattered radiation (E_{SC}) from the tip−sample junction is collected by the same objective lens and coherently amplified (homodyned) with the strong (at least $\sim 5 \times E_{SC}$) reference beam (E_{ref}) in the output port of the interferometer, which is focused onto the silicon photodiode and the CCD camera (for alignment purposes). The signal from the photodiode is demodulated by a lock-in amplifier (Signal Recovery, model 7280) at the harmonics (Ω, 2Ω, or 3Ω) of the cantilever dithering frequency, Ω. For the acquisition of the ANSOM images, the same line is scanned twice with two reference-beam phases differing by $\pi/2$ (Γ_1 and $\Gamma_2 = \Gamma_1 + \pi/2$) and stored separately in the computer. The two images with different phases are later processed offline to extract the ANSOM intensity ($I_{n\Omega}$) according to the following relation:

$$I_n = |E_n|^2 = |E_{NF,n\Omega}|^2 \propto [S_{n\Omega}(\Gamma_1)]^2 + [S_{n\Omega}(\Gamma_1 + \pi/2)]^2 \quad (5)$$

No other postprocessing of the images was carried out except for the correction of the sample plane tilt in the AFM topography image. The feedback loop is temporarily disabled while recording the approach curve (signal as a function of the tip−sample distance), and the computer stops the approach when the cantilever tapping amplitude becomes smaller than the preset value.

Nitride samples are epitaxial thin films grown by plasma-assisted molecular beam epitaxy (MBE) on sapphire (0001) substrates. GaN films are grown with a nitrogen/Ga flux ratio close to 1, which obtains a smooth surface morphology and avoids accumulation of metallic Ga droplets as well. These GaN films are also used as the templates for InN growth, where more nitrogen is supplied than indium, such that the formation of indium droplets is completely suppressed. The resultant InN films are composed of small mesalike islands with flat (0001) tops. Details of the growth are reported elsewhere.[19]

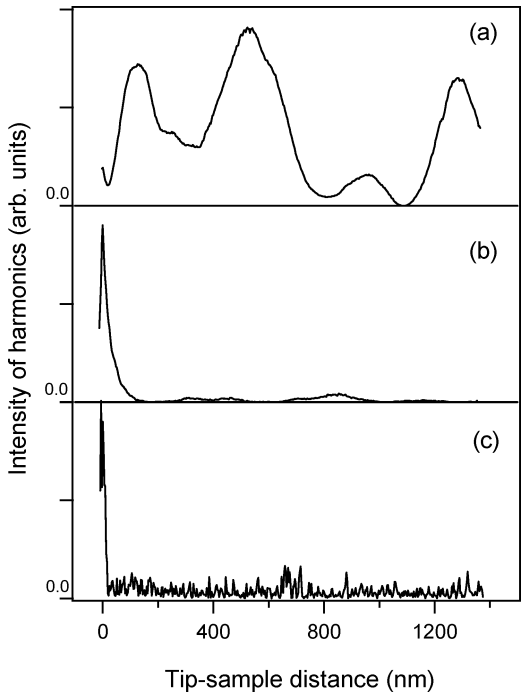

Figure 2. Demodulated signals (intensities) as a function of the tip−sample distance: (a) fundamental, (b) second harmonic, and (c) third harmonic. The tip is above an InN island grown on top of a GaN layer. The zero tip−sample distance is defined as the point at which the tapping amplitude shows appreciable damping. The decrease in the signal after tip−sample contact (negative tip−sample distance) is due to a decrease in the tapping amplitude.

Results and Discussion

a. Characterization of the Near-Field Signal. The amount of the perturbation of the optical polarizabilities of the tip and sample surfaces decays rapidly with the tip−sample distance. Therefore, the near-field scattering signal should show a fast decay upon increasing the tip−sample distance, whereas the far-field background is either constant or oscillatory on the length scale of the wavelength. The oscillatory background leads to the topography-related artifacts in ANSOM images, and these need to be filtered out from the signal. In Figure 2, we plot the homodyne-amplified signal (intensity) as a function of the tip−sample distance detected at the fundamental, second, and third harmonic frequencies of the cantilever oscillation. The sample used is an InN thin film grown on a GaN surface (see the next section for further characterization of the sample). The zero sample−tip distance is defined as a point at which the tapping amplitude shows abrupt damping. The fundamental signal (Ω) is dominated by the oscillatory background that originates from the interference between the sample surface and tip scattering. As we move to higher harmonic signals, the oscillatory background starts to disappear, and finally, for the third harmonic signal (3Ω), the far-field background is completely reduced below the noise level of the detector. In the following, we use only the third harmonic signals that have no far-field background.

Figure 3 shows the short-range tip−sample distance dependence of the third harmonic intensity signal ($I_3 = |E_3|^2$) along with a simulated signal based on the coupled dipole model (see below). The near-field scattering decays completely within 20 nm from the sample surface, showing the extremely localized nature of the tip−sample coupling. To gain insight into the near-field coupling mechanism, we carried out a simulation based on the quasi-electrostatic dipole-coupling model[17] in which the

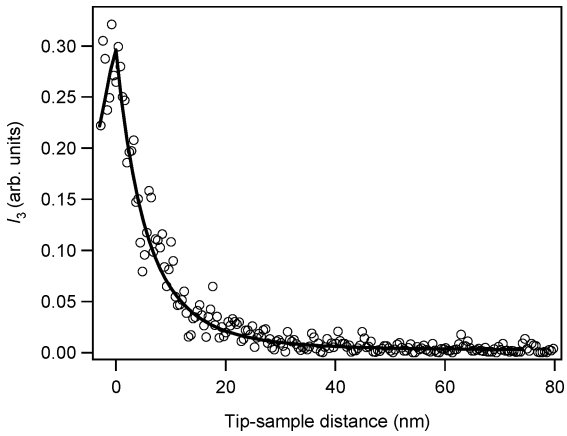

Figure 3. Comparison of the third harmonic intensity (I_3) signal (empty circles) above an InN island and the simulation (solid lines) based on the dipole-coupling model (see text). The simulated curve includes a constant offset of the signal to take into account the constant noise of the actual signal.

tip end is approximated as a point dipole interacting with its own image generated by the sample surface. Within the quasi-electrostatic dipole approximation, the effective polarizability of the tip−sample system is given as[17]

$$\alpha_{\text{eff}}(z) = \frac{\alpha(1+\beta)}{1 - \dfrac{\alpha\beta}{16\pi(z+a)^3}} \tag{6}$$

where z is the distance between the sample and the tip end and a is the radius of the tip end. In this model, the spatial and temporal variation of the optical phase (phase retardation) within the tip−sample system is ignored because of the subwavelength size of the system (quasi-electrostatic approximation). The quantity α is the unperturbed polarizability of the tip end [$\alpha = 4\pi a^3(\epsilon_t - 1)/(\epsilon_t + 2)$] and β is the p-polarized Fresnel coefficient of the sample [$\beta = (\epsilon_s - 1)/(\epsilon_s + 1)$], where ϵ_t and ϵ_s are the bulk complex dielectric constants of the tip end and the sample just below the tip, respectively. The near-field scattering amplitude is linearly proportional to the effective polarizability, α_{eff}.[20] From eq 6, it can be shown that the decay length of the near-field scattering is approximately proportional to $a\{[(\epsilon_s - 1)/(\epsilon_s + 1)][(\epsilon_t - 1)/(\epsilon_t + 2)]\}^{1/3}$. Therefore, the tip−sample distance is mostly governed by the effective radius of the tip, although there exists a slight dependence on the dielectric constants of the tip and sample. The demodulated nth harmonic intensity signal is numerically calculated by Fourier transforming the modulated effective polarizability:

$$Q_n(z) = \left| \frac{1}{2\pi} \int_0^{2\pi} \alpha_{\text{eff}}[z + \delta(z)\cos\phi] \exp(in\phi)\, \mathrm{d}\phi \right|^2 \tag{7}$$

where z is the average tip−sample distance and $\delta(z)$ is the amplitude of tip oscillation for a given z. The value of ϕ is the instantaneous phase of tip oscillation. In the limit $\delta(z) \ll$ wavelength employed, the nth harmonic demodulation corresponds to the nth-order derivative of the signal with respect to the tip−sample distance z.

Using eqs 6 and 7 together with the available dielectric constants of the tip and sample,[21−23] we simulated the third harmonic signal as a function of the distance, and the results are compared with the data in Figure 3. For this particular tip, a satisfactory fit to the data could be obtained with an effective tip radius $a = 60$ nm, which is in qualitative agreement with the geometric radius of curvature of the tip, ~50 nm.[24] From

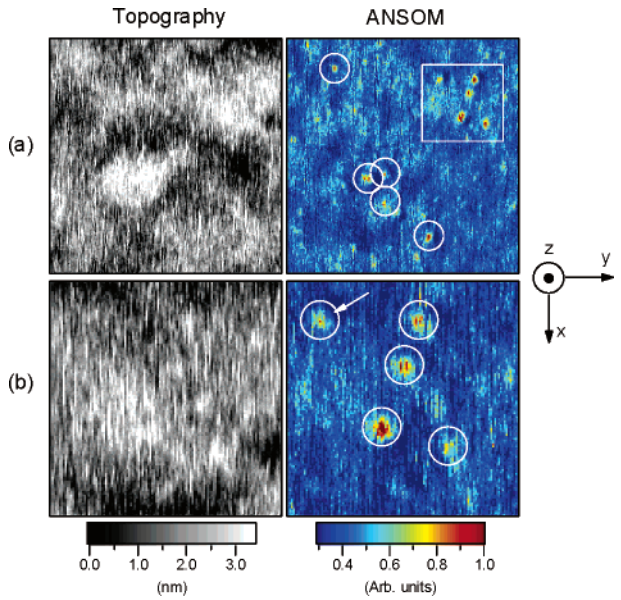

Figure 4. AFM and ANSOM (third harmonic intensity) images. (a) 2 × 2 μm scans. Bright spots (see the text) are marked with circles and a box. (b) Enlarged scans (700 × 700 nm) of the region marked by a square in part a. The arrow points to the bright spot used for estimating the spatial resolution. Also shown is the coordinate system with respect to the illumination direction (see Figure 1).

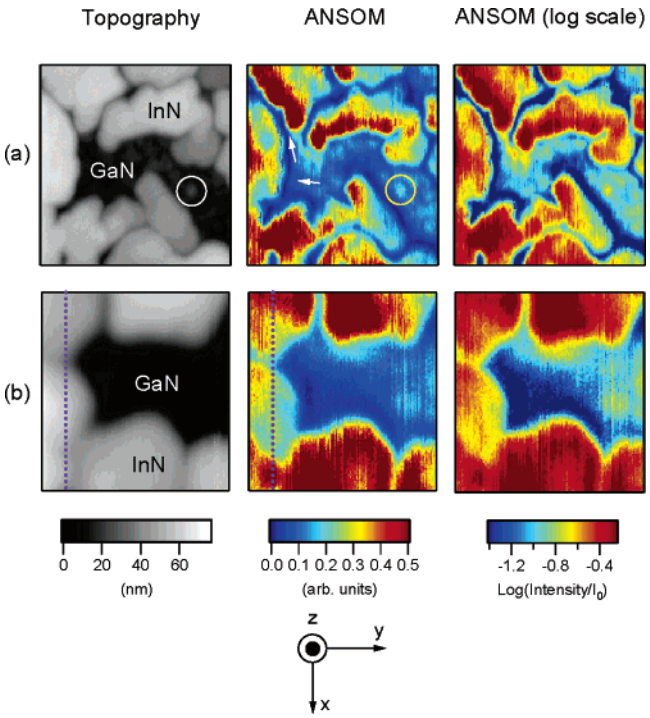

Figure 5. Two selected regions of the AFM, ANSOM (third harmonic, linear color scale) intensity, and ANSOM (third harmonic, logarithmic color scale) intensity images of the InN/GaN sample: (a) 1.3 × 1.3 μm; (b) 400 × 400 nm. The intensity variation within InN islands, and between the islands, is substantial (more than 70% of the maximum contrast within an image), and a simple linear color-scale representation obscures the overall image contrast between the InN islands and the underlying GaN film. Therefore, we show both saturated (50% of the maximum signal) linear-color-scale (second column) and logarithmic-scale (third column) images. The white arrows point to the features from the edge-darkening effect (see the text). Circles indicate the structure within GaN films. Dashed lines (purple) in Figure 4b indicate the position of the line profile shown in Figure 6. Also shown is the coordinate with respect to the illumination direction (see Figure 1).

repeated experiments with different tips, we find that the model slightly, yet consistently, overestimates the actual tip radius by a factor of 1.2−2. A similar behavior was recently observed by Stebounova et al.[25] in infrared ANSOM. We attribute this difference between the effective tip radius and the geometric tip radius to the far-field antenna effect of the inverted metal cone structure surrounding the spherical tip end.[26] In this regard, the effective radius of the tip (a) does not necessarily represent the spatial resolution achievable in ANSOM. Rather, the effective tip radius is a measure of the field localization around the tip end.

b. ANSOM Imaging of GaN and InN. Figure 4 shows two selected AFM topography and ANSOM images (third harmonic intensity) of epitaxially grown GaN films (∼150 nm thickness) on sapphire substrates. From the AFM images in Figure 4a, we find that the root-mean-square variation in the AFM topography is less than 1 nm over a 2 × 2 μm range. Visible structures with an ∼700 nm diameter in the topography originate from the typical hill-and-valley morphology in MBE-grown GaN films.[27] The corresponding ANSOM image shows a reasonably uniform (average contrast variation of less than 16%) intensity distribution over the scanning range, indicating that the GaN film has a homogeneous dielectric (refractive) environment. However, a close examination of the ANSOM image reveals several bright spots (marked with circles and a box) above the uniform intensity distribution. In Figure 4b, we show the results of a zoom-in scan (700 × 700 nm) of the area marked (box) in Figure 4a. In this image, at least five bright spots with a size (full width at half-maximum) ∼ 60 nm or less can be clearly identified (circles). These bright spots show an intensity contrast of up to 4:1 relative to the neighboring regions. They do not have any noticeable topographic features (protrusions or pits) at the corresponding locations in the AFM image within the feedback noise (∼5 Å) of the AFM. At this point, we are unable to identify the exact nature of these "hot spots" in the GaN films. We hypothesize that they are caused by localized defects in the GaN crystal or inclusions of small (less than 1 nm) metallic Ga droplets, which lead to highly localized dielectric perturbations in the GaN thin film. Using the smallest bright spot in Figure 4b (marked with an arrow), we can estimate the spatial resolution of our ANSOM image. A Gaussian fit (not shown) of the line profile of the feature reveals that the spatial resolution is better than 30 nm. It should be noted again that the spatial resolution of the image does not necessarily correspond to the effective tip radius derived from the tip−sample distance curve. The effective tip radius only represents the overall size of the optically active part of the tip, not the spatial resolution. Also, higher harmonic detection increases the effective resolution by spatial filtering of the spatial frequencies.[17]

Figure 5 shows two selected ANSOM and AFM topography images of InN islands epitaxially grown on top of a flat GaN film similar to the film shown in Figure 4. In the AFM images, the InN islands are characterized by mesalike islands of 100−500 nm diameter and ∼50 nm height. The ANSOM can distinguish the InN islands from the underneath GaN layer: the InN islands exhibit a strong positive contrast compared to the GaN layer, and the spatial resolution is better than 50 nm. Also observable in the ANSOM image of Figure 5a are similar structures within the exposed region of the GaN film caused by the local refractive-index variation, as seen in Figure 4.

The larger refractive index of InN relative to GaN induces a stronger image dipole of the tip, which increases the overall scattering efficiency. It should be noted that the scattering efficiency and, hence, the image contrast are determined by both

the real (refractive) and the imaginary (absorptive) parts of the dielectric constant, and from the image alone, one cannot untangle the real and imaginary contributions to the image. The ANSOM image in Figure 5a shows dark lines that closely follow the rims and interfaces of the InN islands (marked with arrows). These dark lines mostly originate from the "edge-darkening" effect:[28] at the rim of sharp objects, or at the centers of narrow pits, the optically active part of the AFM tip (apex) cannot reach the sample surface. Instead, the (optically inactive) facet of the AFM tip images the topography of the sample. Consequently, this leads to an increased distance between the tip end and the sample and, hence, leads to a reduction of the ANSOM signal.

From the image histograms (not shown) of five different images taken in different regions of the sample, we obtain the relative intensity contrast between InN and GaN as 3.6 ± 0.7:1 [the uncertainty corresponds to 1 standard deviation ($1\sigma_{n-1}$) of the contrast ratios of five images]. In establishing the relative contrast, we assign regions with a topographical height larger than 50 nm to be InN islands and the rest of the regions to the GaN film. The contrast is significantly larger than the local spatial variation of the ANSOM signals from the pure GaN films (~16%). A change of the imaging conditions, such as the tapping amplitude and set point, does not change the apparent image contrast, and, hence, we believe that this contrast is not related to any scanning artifact. Using the dipole-coupling model (see eq 6) and the available bulk dielectric constants of InN ($\epsilon = 7.71 + 0.83i$) and GaN ($\epsilon = 4.67 + 0.4 \times 10^{-4}i$)[21−23] at 633 nm, we calculate a theoretical intensity-contrast ratio of 2.1:1. The agreement between the experimental contrast and the dipole-coupling theory is only qualitative, partly because of the simplifying assumptions made in the model. Improved agreement would be achieved by including higher-order corrections to the model, such as the effect of the sample thickness (in our case, the height of the InN island), effects of the underlying substrate, and the inclusion of higher-multipole contributions. Raschkea and Lienau[29] recently showed that the ANSOM signal sensitively depends on the vertical composition of the sample, and they suggested the possible role of higher-order interactions between the tip and the sample.

A close inspection of the ANSOM images of Figure 5 reveals features that do not show up in the corresponding topography. Especially, we notice large variations in the ANSOM intensity within a topographically flat island and between neighboring InN islands. Also, it appears that these intensity variations do not have any apparent correlation with the topography or height of the InN islands. In Figure 6, we show the line profiles of the AFM and ANSOM images shown in Figure 5b (marked with dashed lines). The line profiles span three neighboring InN islands with similar topography (less than 10 nm differences) and shape. However, the InN island in the middle of the profile (displacement = 80−260 nm in Figure 6) appears noticeably darker than the other two neighboring islands.

One possible source of the extra structure and intensity variation is the direct excitation of the sample dipole.[30,31] When the sizes of the objects (or local features in a larger structure) are similar to or smaller than the dimension of the tip, the object can no longer act as a simple flat dielectric mirror that generates a simple mirror dipole of the tip. Instead, the dipole of the object can be directly excited by the illumination and the excited sample dipole interacts with the tip−dipole moment. In this situation, the ANSOM images not only probe the local dielectric environment of the object but also probe the local field distribution directly above the sample. Therefore, the image contrast will be influenced by effects such as the illumination

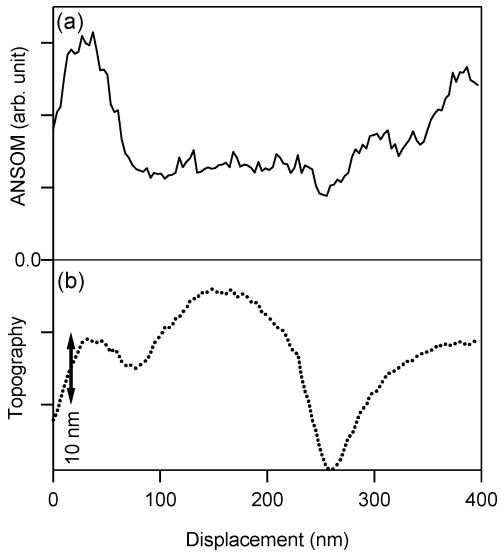

Figure 6. Line profiles of the (a) ANSOM and (b) AFM images of Figure 5b (dashed lines in Figure 5b).

direction and the detailed topography of the sample. Also, at the edges of the object, the image−dipole model will be a less rigorous approximation to the real tip−sample interaction and the ANSOM image may significantly deviate from the topographic distribution of the material. An alternative explanation to the extra structures can be given in terms of the local microscopic variation of the dielectric environment within the InN islands. It is known[32,33] that the bulk optical properties (such as the band-gap and dielectric constants) of InN crystals are critically dependent on the growth conditions, because of the possible variations in the internal mechanical strain, chemical impurities, or local defects. Therefore, it is possible that the extra structures in the ANSOM images of the InN islands are a reflection of the distributions of defects or chemical impurities, which affect the local dielectric environment.

Conclusion and Summary

In this work, we successfully imaged and identified epitaxially grown GaN and InN semiconductor thin films using the ANSOM technique, showing the prospects for the application of ANSOM to a greater variety of semiconductor systems with nanometric spatial resolution. We found that major features of the tip−sample interaction and the image contrast could be satisfactorily explained by a simple dipole-coupling model. At the same time, however, we found that the dipole-coupling model is not sufficient to explain all of the detailed features in the ANSOM images. With a refined model that takes into account other factors such as the phase retardation, higher-order multipole effects, and underlying substrate effects, we will be able to explain more of the features appearing in the high-resolution ANSOM images.

Acknowledgment. The authors gratefully acknowledge the support from the National Science Foundation under Grant NSF-DMR-0302446 and from the U.S. Department of Energy under Contract DEAC03-76SF00098 for the construction of the laboratories, additional equipment, and support of the InN/GaN growth studies. The authors thank Dr. Fritz Keilmann for helpful discussions and Jan Preusser and Sandra Börner for assistance in the development of the instrumental setup. Parts of the equipment are on loan from the National Institute of Standards and Technology.

References and Notes

(1) Betzig, E. *Science* **1991**, *251*, 1468.
(2) Betzig, E.; Trautman, J. K. *Science* **1992**, *257*, 189.
(3) Pohl, D. W.; Denk, W.; Lanz, M. *Appl. Phys. Lett.* **1984**, *44*, 651.
(4) Hecht, B.; Sick, B.; Wild, U. P.; Deckert, V.; Zenobi, R.; Martin, O. J. F.; Pohl, D. W. *J. Chem. Phys.* **2000**, *112*, 7761.
(5) Knoll, B.; Keilmann, F. *Nature* **1999**, *399*, 134.
(6) Hillenbrand, R.; Keilmann, F. *Phys. Rev. Lett.* **2000**, *85*, 3029.
(7) Zenhausern, F.; Martin, Y.; Wickramasinghe, H. K. *Science* **1995**, *269*, 1083.
(8) Hartschuh, A.; Sanchez, E. J.; Xie, X. S.; Novotny, L. *Phys. Rev. Lett.* **2003**, *90*, 095503.
(9) Ichimura, T.; Hayazawa, N.; Hashimoto, M.; Inouye, Y.; Kawata, S. *Appl. Phys. Lett.* **2004**, *84*, 1768.
(10) Sanchez, E. J.; Novotny, L.; Xie, X. S. *Phys. Rev. Lett.* **1999**, *82*, 4014.
(11) Stöckle, R. M.; Suh, Y. D.; Deckert, V.; Zenobi, R. *Chem. Phys. Lett.* **2000**, *318*, 131.
(12) Pankov, J. I.; Moustakas, T. D. *Gallium Nitride (GaN) I, Semiconductors and Semimetals*; Academic Press: San Diego, CA, 1998; Vol. 50.
(13) Hillenbrand, R.; Keilmann, F. *Appl. Phys. Lett.* **2002**, *80*, 25.
(14) Furukawa, H.; Kawata, S. *Opt. Commun.* **1998**, *148*, 221.
(15) Aigouy, L.; Lahrech, A.; Gresillon, S.; Cory, H.; Boccara, A. C.; Rivoal, J. C. *Opt. Lett.* **1999**, *24*, 187.
(16) Maghelli, N.; Labardi, M.; Patane, S.; Irrera, F.; Allegrini, M. *J. Microsc. (Oxford)* **2001**, *202*, 84.
(17) Knoll, B.; Keilmann, F. *Opt. Commun.* **2000**, *182*, 321.
(18) Azoulay, J.; Debarre, A.; Richard, A.; Tchenio, P. *Appl. Opt.* **2000**, *39*, 129.
(19) Liu, B.; Kitajima, T.; Chen, D.-X.; Leone, S. R. *J. Vac. Sci. Technol., A* **2005**, in press.
(20) Bohren, C. F.; Huffman, D. R. *Absorption and Scattering of Light by Small Particles*; John Wiley & Sons: New York, 1998.
(21) Jiang, L. F.; Shen, W. Z.; Yang, H. F.; Ogawa, H.; Guo, Q. X. *Appl. Phys. A* **2004**, *78*, 89.
(22) Wolos, A.; Palczewska, M.; Zajac, M.; Gosk, J.; Kaminska, M.; Twardowski, A.; Bockowski, M.; Grzegory, I.; Porowski, S. *Phys. Rev. B: Condens. Matter Mater. Phys.* **2004**, *69*, 115210.
(23) Yu, G.; Ishikawa, H.; Egawa, T.; Soga, T.; Watanabe, J.; Jimbo, T.; Umeno, M. *Jpn. J. Appl. Phys.* **1997**, *36*, L1029.
(24) From the data sheet from MikroMasch, we estimate that the radius of curvature of the Pt/Ti-coated tip cannot be better than 10 nm but it can be better than 50 nm.
(25) Stebounova, L.; Akhremitchev, B. B.; Walker, G. C. *Rev. Sci. Instrum.* **2003**, *74*, 3670.
(26) Knoll, B.; Keilmann, F.; Kramer, A.; Guckenberger, R. *Appl. Phys. Lett.* **1997**, *70*, 2667.
(27) Ruterana, P.; Albrecht, M.; Neugebauer, J. *Nitride Semiconductors, Handbook on Materials and Devices*; Wiley-VCH: Weinheim, Germany, 2003.
(28) Taubner, T.; Hillenbrand, R.; Keilmann, F. *J. Microsc. (Oxford)* **2002**, *210*, 311.
(29) Raschkea, M. B.; Lienau, C. *Appl. Phys. Lett.* **2003**, *83*, 5089.
(30) Hillenbrand, R.; Keilmann, F.; Hanarp, P.; Sutherland, D. S. *Appl. Phys. Lett.* **2003**, *83*, 368.
(31) Hillenbrand, R.; Keilmann, F. *Appl. Phys. B* **2001**, *73*, 239.
(32) Wu, J.; Walukiewicz, W.; Shan, W.; Yu, M.; Ager, J. W., III; Haller, E. E.; Lu, H.; Schaff, W. J. *Phys. Rev. B: Condens. Matter Mater. Phys.* **2002**, *66*, 201403.
(33) Shubina, T. V.; Ivanov, S. V.; Jmerik, V. N.; Solnyshkov, D. D.; Vekshin, V. A.; Kop'ev, P. S.; Vasson, A.; Leymarie, J.; Kavokin, A.; Amano, H.; Shimono, K.; Kasic, A.; Monemar, B. *Phys. Rev. Lett.* **2004**, *92*, 117407.